

Electrocatalytic MOF-Carbon Bridged Network Accelerates Li^+ -Solvents Desolvation for High Li^+ Diffusion toward Rapid Sulfur Redox Kinetics

Linge Li, Haifeng Tu, Jian Wang,* Mingchao Wang, Wanfei Li, Xiang Li, Fangmin Ye, Qinghua Guan, Fengyi Zhu, Yupeng Zhang, Yuzhen Hu, Cheng Yan,* Hongzhen Lin, and Meinan Liu*

Lithium-sulfur batteries are famous for high energy density but prevented by shuttling effect and sluggish electrochemical conversion kinetics due to the high energy barriers of Li^+ transport across the electrode/electrolyte interface. Herein, the Li^+ -solvents dissociation kinetics is catalyzed and stimulated by designing a carbon bridged metal-organic framework (MOF@CC), aimed at realizing increased bare Li^+ transport for the rapid conversion kinetics of sulfur species. Theoretical simulations and spectroscopic results demonstrate that the bridged MOF@CC well grants a special transport channel for accelerating Li^+ benefited from aggregated anion/cation clusters. Moreover, the C–N bridge between $-\text{NH}_2$ ligand in MOF and carbon shell enhances electron exchange, and thus promotes polysulfide catalytic efficiency and hinder polysulfide aggregation and accumulation. With the MOF@CC-modified separators, the assembled Li/S batteries deliver a reversible capability of 1063 mAh g^{-1} at 0.5 C, a capacity retention of 88% after 100 cycles, and a high-rate performance of 765 mAh g^{-1} at 5 C. Moreover, the large areal pouch cell with $100 \mu\text{m}$ Li foil and lean electrolyte is capable of stabilizing 855 mAh g^{-1} after 70 cycles. These results well demonstrate the efficiency of catalyzing desolvation for fast Li^+ transport kinetics and the conversion of polysulfides.

1. Introduction

With the rapid development of portable electronic devices and electric vehicles, lithium-ion batteries (LIBs) are of difficulty to meet the ever-growing demand on high energy density due to the limited theoretical capacity of cathode/anode (such as LiCoO_2 : 274 mAh g^{-1} , Graphite: 370 mAh g^{-1}).^[1] Thanks to the ultra-high theoretical capacity (1675 mAh g^{-1}) and specific energy density (2600 Wh kg^{-1}), lithium-sulfur (Li/S) batteries have been considered as the promising rechargeable battery systems with lower environmental pollution and material cost.^[2] However, the serious “shuttle effect” and sluggish kinetics of sulfur reduction and sulfide oxidation reactions lead to low utilization and rapid capacity loss, seriously impeding the practical application of Li/S batteries.^[3] In the past ten years, researchers had focused on physically

L. Li, H. Tu, X. Li, Q. Guan, F. Zhu, Y. Zhang, Y. Hu, H. Lin, M. Liu
School of Nano-Tech and Nano-Bionics
University of Science and Technology of China
Hefei, Anhui 230026, China
E-mail: mnliu2013@sinano.ac.cn

L. Li, H. Tu, J. Wang, X. Li, Q. Guan, F. Zhu, Y. Zhang, Y. Hu,
H. Lin, M. Liu
Key Laboratory of Multifunctional Nanomaterials and Smart
Systems & i-lab, Suzhou Institute of Nano-Tech and Nano-Bionics
Chinese Academy of Sciences
Suzhou, Jiangsu 215123, China
E-mail: jian.wang@kit.edu

J. Wang
Helmholtz Institute Ulm (HIU)
89081 Ulm, Germany

 The ORCID identification number(s) for the author(s) of this article can be found under <https://doi.org/10.1002/adfm.202212499>.

© 2023 The Author(s). Advanced Functional Materials published by Wiley-VCH GmbH. This is an open access article under the terms of the Creative Commons Attribution License, which permits use, distribution and reproduction in any medium, provided the original work is properly cited.

DOI: 10.1002/adfm.202212499

M. Wang
Centre for Theoretical and Computational Molecular Science,
Australian Institute for Bioengineering and Nanotechnology
University of Queensland
St Lucia, QLD 4072, Australia

W. Li
School of Materials Science and Engineering
Suzhou University of Science and Technology
Suzhou, Jiangsu Province 215009, China

F. Ye
Center for Optoelectronic Materials and Devices
Key Laboratory of Optical Field Manipulation of Zhejiang Province
Zhejiang Sci-Tech University
Hangzhou 310018, China

C. Yan
School of Mechanical
Medical and Process Engineering
Queensland University of Technology
Brisbane, QLD 4000, Australia
E-mail: c2.yan@qut.edu.au

M. Liu
Division of Nanomaterials and Jiangxi Key Lab of Carbonene Materials
Jiangxi Institute of Nanotechnology
Nanchang 330200, China

confining/shielding the lithium polysulfides (LPSs) and chemically trapping LiPSs. However, the above adsorption strategies work well at the beginning step but they will fail after a certain number of cycling.^[4] The main reason may be attributed to the poor Li⁺ kinetics in diffusion and desolvation processes as well as the sluggish conversions of sulfur species, which leads to heavy LPSs accumulation and finally deactivates all trapping centers.^[5]

As well known, Li ion behaviors in the interface or cathode interior play the decisive role in electrochemical performances. In general, Li ion is typically coordinated with solvent molecules to form solvent-separated ion pairs (SSIPs) complex in most liquid electrolytes.^[6] While the radius of these solvated Li⁺-solvents complex is much larger than that of anions, such as PF₆⁻, TFSI⁻. Consequently, the diffusion rate of Li⁺-solvents complex is lower than that of anions owing to the effect of steric hindrance, reflected by the low transference number of Li⁺ (< 0.4).^[7] Recently, it has been found that Li⁺ solvation structure can affect Li⁺ kinetics significantly by modulating outer anion-involved solvation sheath (reducing the coordinated/solvated solvent molecules in solvation sheath), especially these aggregated ion pairs (AGG, anions interacting with two or more Li⁺), forming a special ion transport channel to facilitate Li⁺ motion.^[8] Another way is to directly separate solvent molecules from the Li⁺-solvents complex and make Li⁺ desolvation process easier. For example, a metal-organic framework (MOF) modified electrolyte was developed by Zhou et al., in which solvent molecules can be sieved by MOF with suitable pore size to get free Li⁺.^[9] These “free” Li⁺ obtained from the Li⁺-solvents complex will benefit the subsequent redox reaction.

On the other hand, the sluggish sulfur/sulfide reaction kinetics are another big challenge owing to the depressive ion transport. Very recently, single atomic catalysts (SACs) have been considered to propel the ion diffusion for enhancing this sluggish conversion kinetics in Li/S system.^[10] For example, Wang et al. used single Fe or Cobalt atoms on propelling lithium ion diffusion for reducing the delithiation barrier of Li₂S, and thus accelerating the reversible electrochemical reactions between Li₂S and LPSs as well as sulfur.^[11] However, synthesis of stable SACs with high yielding amount is jet challenging and uncontrollable. As known, the catalytic efficiency requires elaborative interface connection design to enhance ion and electron transport. Therefore, the improvement of MOF can be solved by constructing quick responses of ion and electron exchange via the bridged transport networks.^[12] Considering the effect of MOF on sieving solvent molecules, the modified MOF with catalytic functions is desired to enhance the kinetics of both Li⁺ diffusion and LPSs conversion.

In this work, a catalytic composite by bridging NH₂-UIO-66 with composite carbon (MOF@CC) is synthesized and coated on polypropylene separator (MOF@CC@PP) for promoting Li⁺ diffusion kinetics resulted from Li⁺-solvents complex and LPSs conversion kinetics in L/S batteries. As illustrated in Figure 1a, Li⁺ ions are mostly surrounded by large amounts of organic ether solvents in bulk solution. The sluggish transport kinetics of large solvated Li⁺ ions slow down the redox conversion among sulfur species. With the introduction of MOF@CC, some coordinated solvent molecules can be sieved and the solvation structure of Li⁺ turns into anion-involved modes, such as

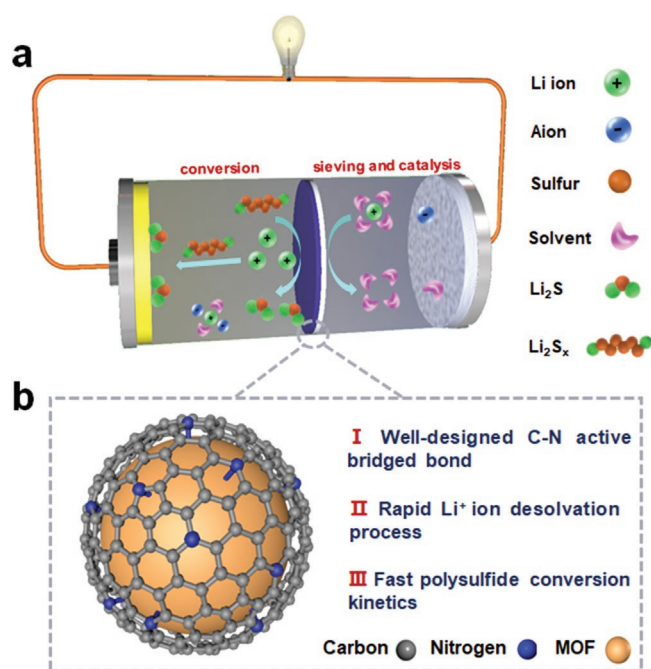


Figure 1. a) Schematic illustration of solvated Li⁺ from bulk solution to MOF@CC@PP surface as well as the redox reactions between polysulfides and formed Li⁺ ions. b) C–N active bridged bond between MOF particles and carbon layer.

contact ion pairs (CIPs) and AGGs. These CIPs and AGGs will fasten Li⁺ diffusion rate, and then promptly bring these naked Li⁺ to reaction sites, thus avoiding the accumulation of LPSs. Meanwhile, the C–N bridged bond in MOF@CC structures are constructed by “welding” highly conductive carbon layer and MOF particles together (Figure 1b), providing the pathway of electronic exchange for high catalytic efficiency. Consequently, although there are some polysulfides shuttles into electrolyte, it will be trapped by MOF@CC and takes electrochemical reaction with the bare Li⁺ from Li⁺-solvent complex under the assistance of electrons from the C–N bridge between MOF and carbon. Thanks to the bifunctional MOF@CC@PP, the fabricated Li/S batteries demonstrate superior reaction kinetics and better rate performance than the controlled ones. The cell modified with MOF@CC@PP has a capacity of 1200 mAh g⁻¹ at 0.2 C and 765 mAh g⁻¹ at 5 C, while PP modified cell only has 739 mAh g⁻¹ at 0.2 C and 510 mAh g⁻¹ at 5 C. More surprisingly, the large areal pouch cell can stabilize a capacity of 855 mAh g⁻¹ after 70 cycles, demonstrating the enhanced Li⁺ diffusion and LPSs conversion kinetics by the catalytic MOF@CC layer.

2. Results and Discussion

The synthesis process of MOF@CC is illustrated in Figure S1 (Supporting Information). Firstly, the metal-organic framework (MOF) was prepared by the reaction between ZrCl₄ and 2-aminoterephthalic acid. The as-prepared MOF mixed with glucose and graphene oxide (GO) solution at 60 °C to form homogeneous suspension (detailed mass ratio can be found in supporting information). Then MOF@GO@glucose composite

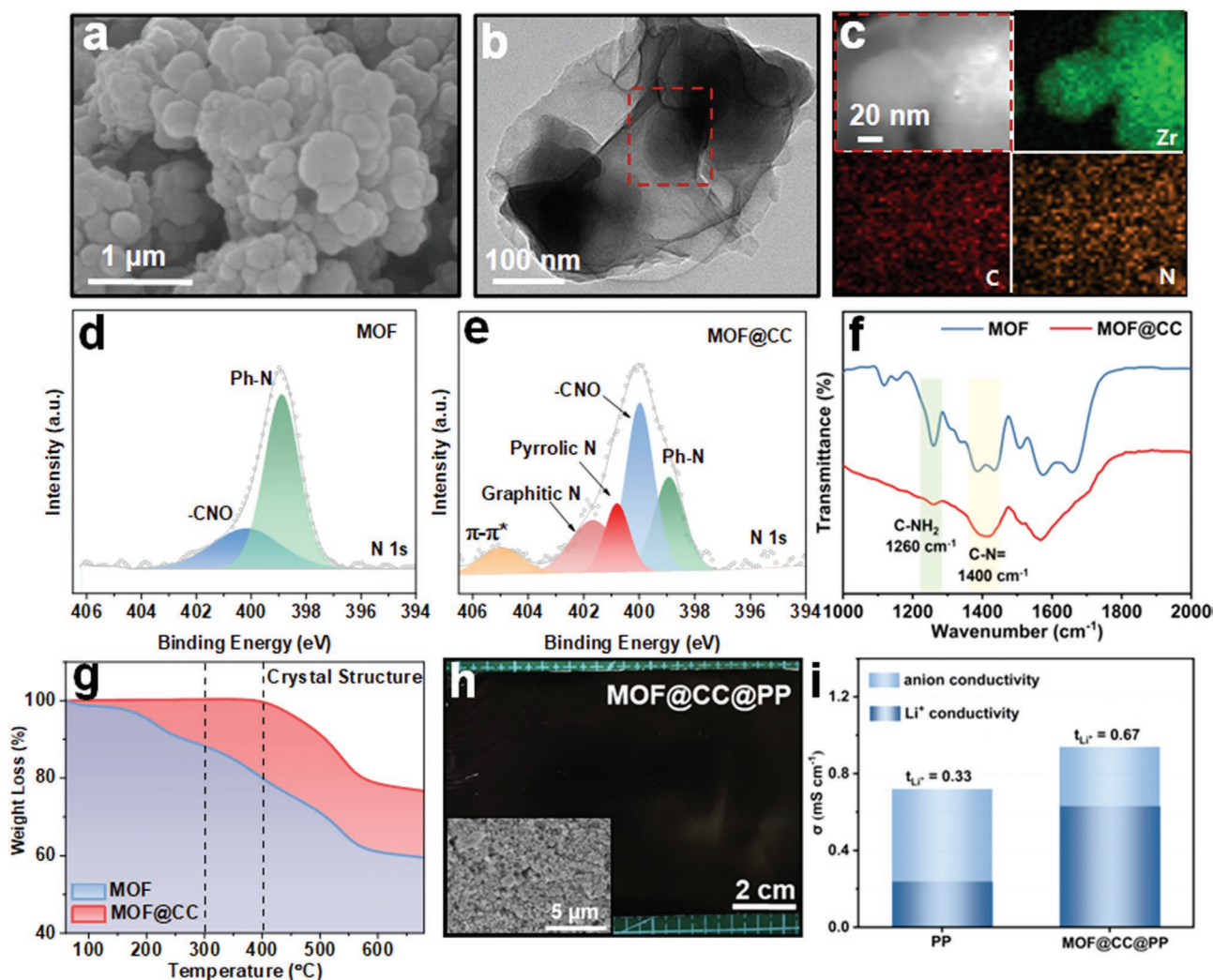


Figure 2. Characterizations of MOF@CC and C–N bridged bond. a) SEM image of MOF@CC. b) TEM image of the MOF@CC and c) corresponding EDX mappings of Zr, C, and N elements. XPS spectra of N 1s in the d) MOF and e) MOF@CC. f) FTIR spectra of MOF and MOF@CC. g) Thermogravimetric curves of MOF and MOF@CC. h) Optical and SEM images of MOF@CC@PP with a scaled size. i) Ionic conductivity and Li⁺ transfer number of PP separator and MOF@CC@PP.

was obtained after evaporating the water; through heating this composite at 350 °C in Ar to finally achieve MOF@CC. In this design, the adopted glucose acts as the carbon precursor. As shown in Figure S2 (Supporting Information), the CC is mainly contributed by the carbonized glucose, which accounts for 92.8% of the mass in CC. While considering the depressive electrical conductivity of carbonized glucose, graphene oxide was also introduced here to form a uniform 3D conductive network for effectively shortening electronic pathways. The as-obtained MOF@CC was coated on the commercial polypropylene (PP, Celgard 2325) to form the final MOF@CC@PP membrane. The structural information of the as-obtained MOF and MOF@CC samples was investigated by a series of characterization methods. As shown in X-ray powder diffraction (XRD) patterns (Figure S3, Supporting Information), the MOF@CC well remains the crystal structure of pure NH₂-UIO-66 even after heating treatment; but simultaneously, amorphous carbon peak at 21° appears, suggesting that CC

may well wrap MOF.^[13] To further reveal the microstructure of MOF@CC, scanning electron microscopy (SEM), transmission electron microscopy (TEM), and aberration transmission electron microscopy (AC-TEM) were used. As shown in Figure 2a, MOF@CC particles show much rougher surface than that of pure MOF particles (Figure S4, Supporting Information), however, it is hard to tell the carbon shell. While TEM and AC-TEM results clearly reveal that these MOF particles are well wrapped by carbon sheets (Figure 2b; Figure S5, Supporting Information). The selected energy-dispersive X-ray spectroscopy (EDS) mapping results confirm that MOF disperses in the core and carbon layer disperses in the shell (Figure 2c). The N element also appears in the wrapped carbon shell, suggesting the formation of C–N bridge resulted from the reaction between MOF ligands and nanocarbon during the heating process (Figure 2c).

The information of the formed C–N bridges in the MOF@CC was further investigated by X-ray photoelectron spectroscopy (XPS), Fourier transform infrared (FTIR) and

Thermogravimetric analysis (TGA). In the high-resolution the N 1s spectrum, compared with the purified MOF, two new peaks (400.8, 401.7 eV) appear in the N 1s spectrum of the MOF@CC sample, corresponding to pyrrolic N and graphitic N, respectively (Figure 2d,e).^[14] These pyrrolic N and graphitic N should be assigned to the C–N bridged bond formation. Meanwhile, the C 1s spectrum of the MOF sample can be divided into three peaks: C=O, C–N, and C=C, corresponding to 288.3, 286, and 284.5 eV, respectively.^[15] Notably, the intensity of C–N in MOF@CC is much higher than that of MOF, indicating new bridged C–N bonds formed in former (Figure S6a,b, Supporting Information). In addition, the peaks at 182.7 and 185.1 eV in Zr 3d spectrum can be ascribed to the Zr–O and Zr–Zr bonds, confirming the chemical state of Zr⁴⁺ in both samples (Figure S6c,d, Supporting Information).^[16] To further reveal the origin of C–N bond, MOF@Glucose and MOF@GO (obtained by heating the mixed MOF/glucose or MOF/GO at 350 °C in Ar) were also studied by XPS analysis as control samples. As shown in Figure S7 (Supporting Information), the C–N peak can be observed at 286 eV in C 1s spectra in both samples, indicating that -NH₂ ligand could be bonded with C atom in both reduced graphene oxide and carbonized glucose. Furthermore, this C–N bond was also investigated by FTIR. As shown in Figure 2f, the peak at 1400 cm⁻¹ can be assigned to C–N, but it should be noted that there are two peaks in MOF sample, while only one peak in MOF@CC sample. The change from two peaks to one peak well demonstrates the transition of -NH₂ coordination from C-NH₂ to C-NH-C. Moreover, the intensity of C-NH₂ peak at 1260 cm⁻¹ in MOF@CC sample becomes much lower than that in MOF sample, again suggesting less C-NH₂ existence.^[17] In addition, the thermal stability of pure MOF and MOF@CC were also characterized by TGA. As shown in Figure 2g, the pure MOF shows poor thermal stability with continuous weight loss due to the carbonization of NH₂- ligand in the initial 300 °C; while MOF@CC keeps excellent thermal stability without any weight loss before 400 °C, indicating that the -NH₂ ligand has been converted into C–N bridged bond in MOF@CC system. A possible formation mechanism of this C–N bridged bond is proposed and described in Figure S8 (Supporting Information). With the assistance of electrons, these -NH₂ ligands in MOF reacts with carboxyl (-COOH) groups on carbon layer to form -CONH. As a consequence, the C–N bridged bond is well constructed in MOF@CC system.

To achieve the practical application of MOF@CC@PP, its large-scale production is inevitable. As shown in Figure 2h, this MOF@CC@PP can be easily scaled up to 15 × 12 cm² without any blanks, demonstrating its potential in future commercialization. Both the MOF@PP separator and MOF@CC@PP exhibit outstanding flexibility at any angle. The thickness and mass loading of MOF@CC is 5 μm and 0.422 mg cm⁻², respectively (Figure S9, Supporting Information). To value the influence of this MOF@CC layer on the electrolyte wettability, contact angle experiments were performed. As shown in Figure S10 and Movie S1 (Supporting Information), MOF@CC layer shows a high wettability to the electrolyte and the interfacial contact angle is ≈0°, much smaller than that of PP (49°), which will be beneficial for reducing the resistance of Li ion diffusion. As well known, ionic conductivity (σ) and Li⁺

transference number (t_{Li^+}) are key parameters to evaluate the desolvation degree since they determine the efficiency of carrier diffusion and ionic mobilities.^[19] Under the temperature ranging from 273.15 to 353.15 K, the MOF@CC@PP system exhibits much higher ionic conductivity than the one with pure PP separator (Figure S11, Supporting Information). For example, the ionic conductivity in the MOF@CC@PP system is as high as 0.94 mS cm⁻¹ (Figure 2i). As calculated according to the Vincent–Bruce method,^[20] the t_{Li^+} across the MOF@CC@PP separator is ≈0.67 at room temperature, which is two times higher than that of the PP separator (Figure 2i; Figure S12, Supporting Information). The enhanced σ and t_{Li^+} of MOF@CC@PP may be contributed by the unique MOF@PP modified layer. As depicted in Figure 3a, the Li⁺-solvents complex keeps the similar structure when penetrating through PP separator, however these complicated complexes need extra energy to remove the solvent molecules to achieve Li⁺ ions, resulting in huge barriers. In contrast, the outer solvation sheath can be sieved when these large-size solvated Li⁺ ions going through the narrow channel of the MOF@CC layer, and moreover the active C–N bridged bond in MOF@CC structures acts as the catalytic sites to propel the desolvation of inner Li(solvent)_x⁺ with the help of fast electronic injection. Finally, the naked Li⁺ ions can be quickly formed and participate in the sulfur reduction and sulfide oxidation without costing too much energies, accelerating the reaction kinetics (Figure 3b).

To further reveal the working mechanism of this MOF@CC layer on enhanced σ and t_{Li^+} , Raman spectroscopy and the molecular dynamic simulations were performed. Raman samples were prepared by dripping 1 M LiTFSI/DOL/DME liquid electrolyte into PP, MOF@PP, and MOF@CC@PP separators. Moreover, a control sample was also prepared by dripping 3 M LiTFSI/DOL/DME LE into PP separator. Previous work reported that the behaviors of TFSI⁻ in the electrolyte consist of three different dissociation states: free TFSI⁻ at 740 cm⁻¹, contact ion pairs at 745 cm⁻¹ (CIPs, TFSI⁻ interacting with a single Li⁺) and aggregated ion pairs at 750 cm⁻¹ (AGGs, TFSI⁻ interacting with two or more Li⁺).^[21] As shown in Figure 3c and Figure S13 (Supporting Information), the TFSI⁻ main peak is located at 740 cm⁻¹ in PP with 1M electrolyte; while this peak shifts to a higher wavenumber region in MOF@CC, suggesting that TFSI⁻ participates in the coordination with Li⁺, which is similar to that in PP with 3M electrolyte. Through quantitatively analyzing the ratio of three dissociation states in four samples (Figure 3d), it can be found that MOF@CC modified system exhibits the highest total ratios of AGGs+CIPs (99%) among all samples (PP with 1M electrolyte: 54%; MOF: 95%; PP with 3M electrolyte: 97%). These results suggest that MOF@CC plays a role in creating a localized highly concentrated lithium salt electrolyte through desolvation of solvent molecules from Li⁺-solvents complex. Moreover, the coordination structures of Li⁺ and the radial distribution function (RDF) were also calculated via molecular dynamic simulations to further understand the influence of MOF@CC (Figure 3e–g). As shown in Figure 3f, the Li–O peak locates at 2.14 Å ascribed to the interaction between Li⁺ and DME/DOL, which can also be found in the presence of MOF.^[22] It should be noted that the intensity of Li–O peak becomes lower in the presence of MOF, suggesting the changed coordination environment of Li⁺. From the calculated

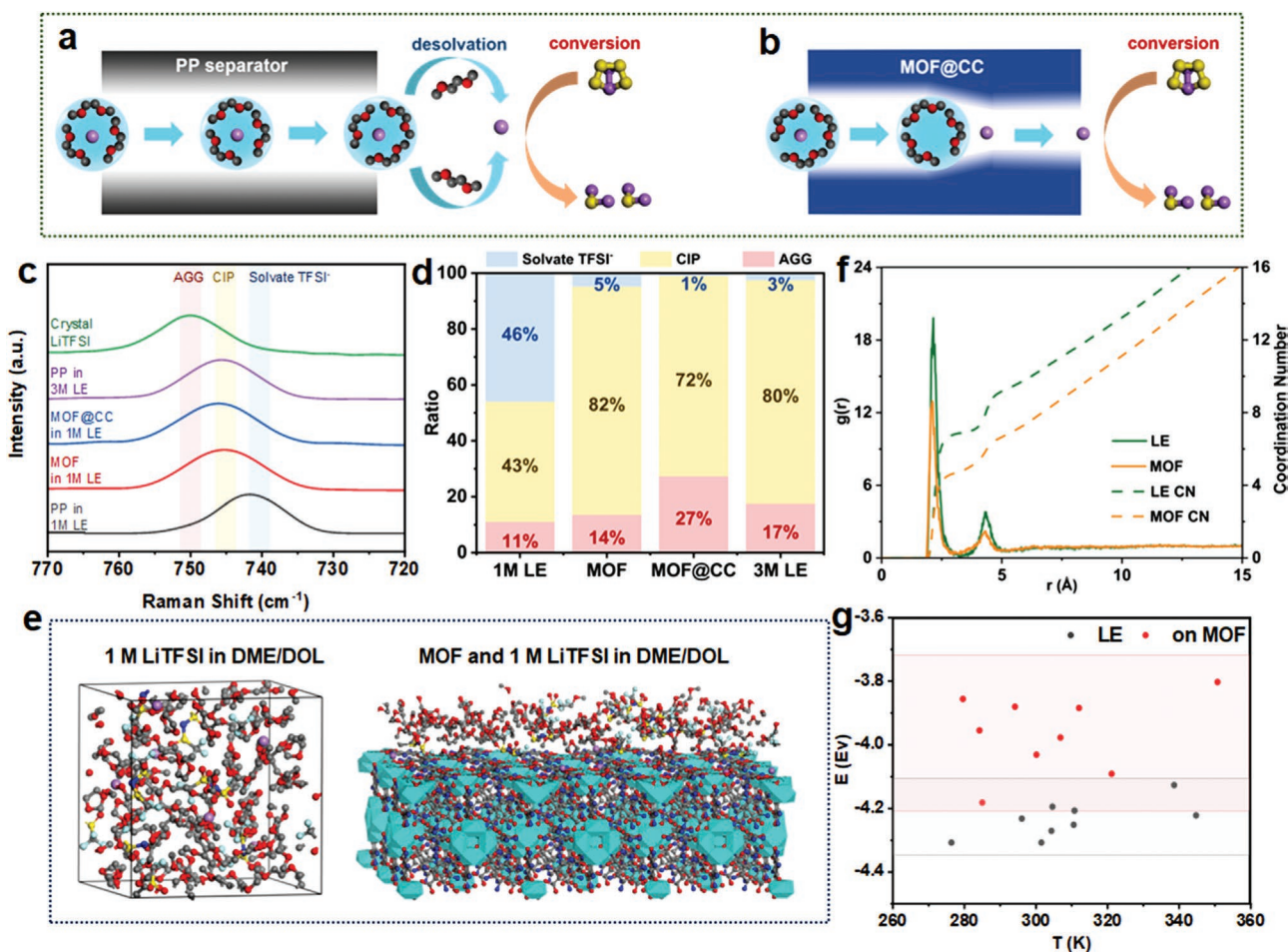


Figure 3. Desolvation kinetics accelerated by MOF@CC bridged network via simulation and spectroscopic experiments. Schematic illustration of solvated Li⁺ ions inside a) a PP separator and b) MOF channels. c) Raman spectra of the various electrolyte with/without MOF@CC. d) The ratio summary of solvated TFSI⁻, CIP, and AGG in different systems. e) Snapshots of commercial electrolyte with/without MOF via MD simulation. Color code: C-dark grey, H-white, O-red, N-blue, F-cyan, S-yellow, Li-purple. f) The radial distribution function and coordination number of Li⁺-O in the commercial electrolyte without/with the presence of MOF. g) Interaction energy between Li⁺ and solvent molecules in the commercial electrolyte with/without MOF.

coordination number (CN) of O atoms in Li⁺-solvents complex, it can be found that the CN drops from 10.4 to 5.2 after introducing MOF in the system. The reduced CN reflects that Li⁺ coordinates with less solvent molecules in MOF system, which will enable the following desolvation easily.^[23] The interaction energy between Li⁺ and solvent molecules, as calculated and summarized in Figure 3g, again demonstrates the lower desolvation energy of MOF system. Based on the above Raman characterization and calculation results, it can be concluded that MOF effectively regulates the solvation structure of Li⁺, reduces the desolvation energy, and thus enhances Li⁺ mobility.

To well investigate the effect of the formed bare Li⁺ ions on the kinetics of the Li/S battery, diffusion coefficients of Li⁺ (D_{Li^+}) in systems with PP, and MOF@CC@PP were measured through CV tests. Moreover, to clarify the function of C-N bridged bond in influencing kinetics, a control sample of MOF mixed with CC, denoted as MOF+CC@PP, was also studied here. As shown in Figure 4a and Figure S14 (Supporting Information), the cathodic reduction peak at R2 is attributed to the reduction of S₈ to high-order Li₂S_x and the reduction R1 corresponds to the further reduction of Li₂S_x to insoluble Li₂S. The

strong oxidation peak at O2 with a shoulder at O1 suggests that Li₂S was gradually converted back to S₈.^[24] With the increase of scanning rates (0.1–0.3 mV s⁻¹), the O1 and O2 peak shifts toward higher voltage; while the R1 and R2 peaks shift toward the lower voltage in all systems. The diffusion coefficient of Li⁺ can be calculated based on the Randles–Sevcik equation^[25] and the MOF@CC@PP exhibits the highest D_{Li^+} value among all these three systems (Figure 4b and Figure S15, Supporting Information). The detailed values were summarized in Table S1 (Supporting Information) and presented in Figure 4c. It can be found that the Li⁺ diffusion rate in MOF@CC@PP system ranks first. The high Li⁺ kinetics in MOF@CC@PP system may be benefit for the fast conversions among sulfur species. Furthermore, the Li₂S precipitation and polysulfide conversion experiment were performed. For better comparison, the CNT current collector was adopted in the symmetric and asymmetric cell systems, as illustrated in Figure 4d. As exhibited in Figure 4e, the precipitation capacity of Li₂S in MOF@CC@PP system is 646 mAh g⁻¹, which is the highest among all these three systems (499 mAh g⁻¹ in MOF+CC@PP, 183 mAh g⁻¹ in PP system). A higher Li₂S precipitation capacity and earlier

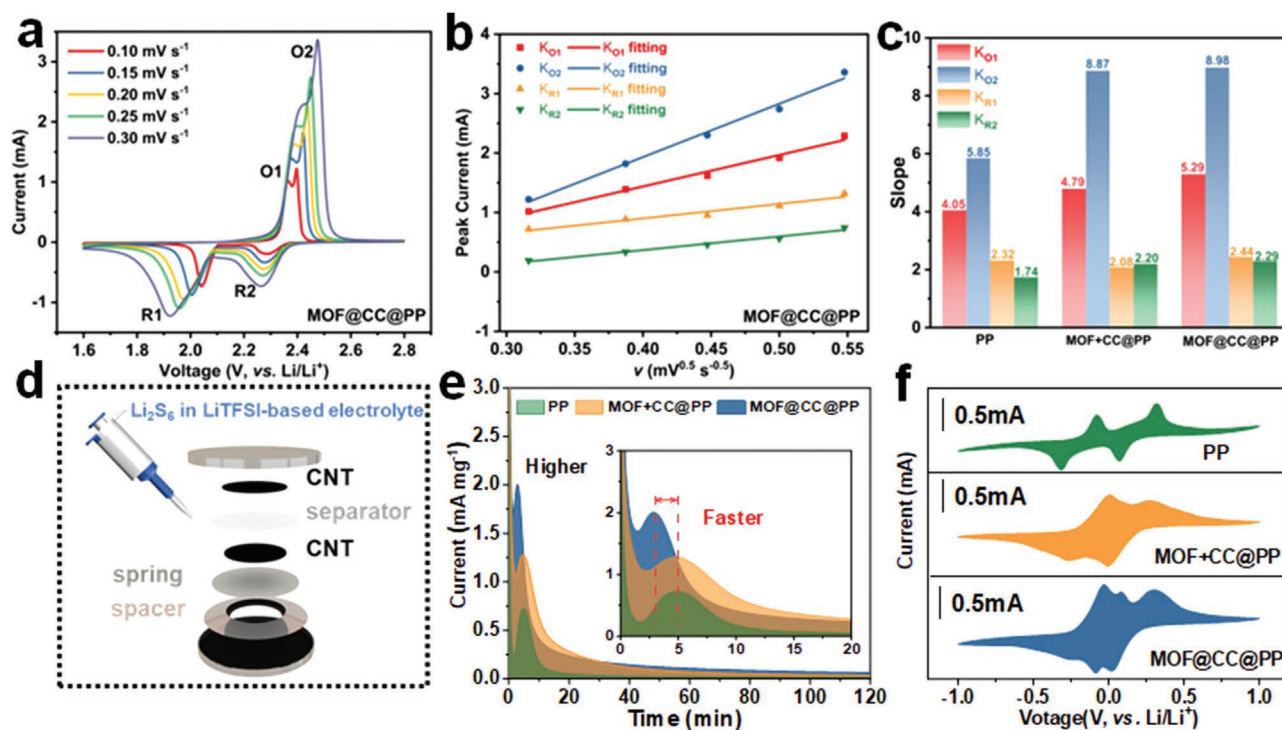


Figure 4. Electrochemical catalytic reaction kinetics improvement by MOF@CC. a) The CV profiles of Li/S cells with MOF@CC@PP from 0.10–0.30 mV s^{-1} . b) Linear fitting of peak currents with Reduction peak R1, Reduction peak R2, oxidation peak O1, and oxidation peak O2 using MOF@CC@PP. c) The corresponding slope histogram. d) Schematic illustration of the CNT/CNT symmetric cells using LiTFSI-based electrolyte with Li_2S_6 dissolved. e) Potentiostatic discharge curves of different separators with Li_2S_6 electrolyte at 2.05 V. f) CV curves of symmetric batteries with Li_2S_6 electrolyte at 0.5 mV s^{-1} .

current response well indicate a faster transformation rate from polysulfides to Li_2S .^[26] Moreover, the CV curves in Figure 4f show a higher redox current and a smaller battery polarization in MOF@CC@PP, again proving its excellent conversion performance.^[27] To directly observe the generated fast lithium ion flux, the symmetric Li/Li cells were assembled to evaluate the interfacial stability of separators against Li anode.^[28] The Li/Li cell with PP separator exhibits rapidly increasing polarization voltage after 360 h, while the Li|MOF@CC@PP|Li cell demonstrates excellent cycling stability over 500 h with lower overpotential at 2 mA cm^{-2} under 1 mAh cm^{-2} , verifying the fast ion diffusion propelled by the MOF@CC (Figure S16, Supporting Information). Besides the fast kinetics of Li^+ enabled by MOF@CC, it also presents effective polysulfide blocking function. As shown in Figure S17 (Supporting Information), MOF@CC@PP well blocks the polysulfide shuttling from left to right chamber in H-typed cell, comparing to commercial PP separator. This block feature may further enhance the cycle stability of Li/S battery.

To demonstrate the effectiveness of the catalytic MOF@CC in improving the performance of Li/S batteries, a series of electrochemical measurements were performed. As shown in electrochemical impedance spectroscopy (EIS) measurements, the charge transfer resistance for MOF@CC@PP is only 38 Ω , lower than that of MOF+CC@PP (44 Ω) and PP (50 Ω), indicating that the MOF@CC@PP exhibits faster charge transfer compared to other separators (Figure S18, Supporting Information).^[29] Benefited from this smaller R_{ct} , MOF@CC@PP

modified Li/S cell is expected to present superior rate performance. Figure 5a displays the Li/S cell with MOF@CC@PP displays a discharge capacity of 1200, 1051, 952, 863, and 765 mAh g^{-1} at 0.2 C, 0.5 C, 1 C, 2 C, and 5 C, respectively. At 5 C, the Li/S cell with PP system only exhibits 510 mAh g^{-1} , much lower than the MOF@CC@PP ones. The voltage profiles in Figure 5b and Figure S19 (Supporting Information) also shows the cell with MOF@CC@PP displays the typical voltage plateaus. Furthermore, the overpotential at different rates for these three systems were summarized in Figure 5c. It can be found that the MOF@CC@PP system shows the lowest overpotential, suggesting the superior kinetics of this system.^[30] For example, the MOF@CC@PP one delivers a higher coulombic efficiency (CE) and the lowest overpotential (293 mV) at 2 C. The cycling stability of the cells was evaluated as well (Figure 5d and Figure S20, Supporting Information). Impressively, the MOF@CC@PP cell delivers an initial discharge capacity of 1063 mAh g^{-1} and the capacity retention can reach as high as 88% (920 mAh g^{-1}) after 100 cycles under 0.5 C; which is much superior to MOF+CC@PP (627 mAh g^{-1}) cell and PP cell (610 mAh g^{-1}). Even under 1 C, the Li|MOF@CC@PP|S cell still shows an outstanding cycling performance and capacity retention (Figure S21, Supporting Information). Meanwhile, the effect of the thickness of the MOF@CC modified layer on electrochemical performance was studied. As shown in Figure S22 (Supporting Information), a thin MOF@CC layer with a thickness of 2 μm could not completely cover PP; while a homogeneous MOF@CC layer with 5 μm on PP can

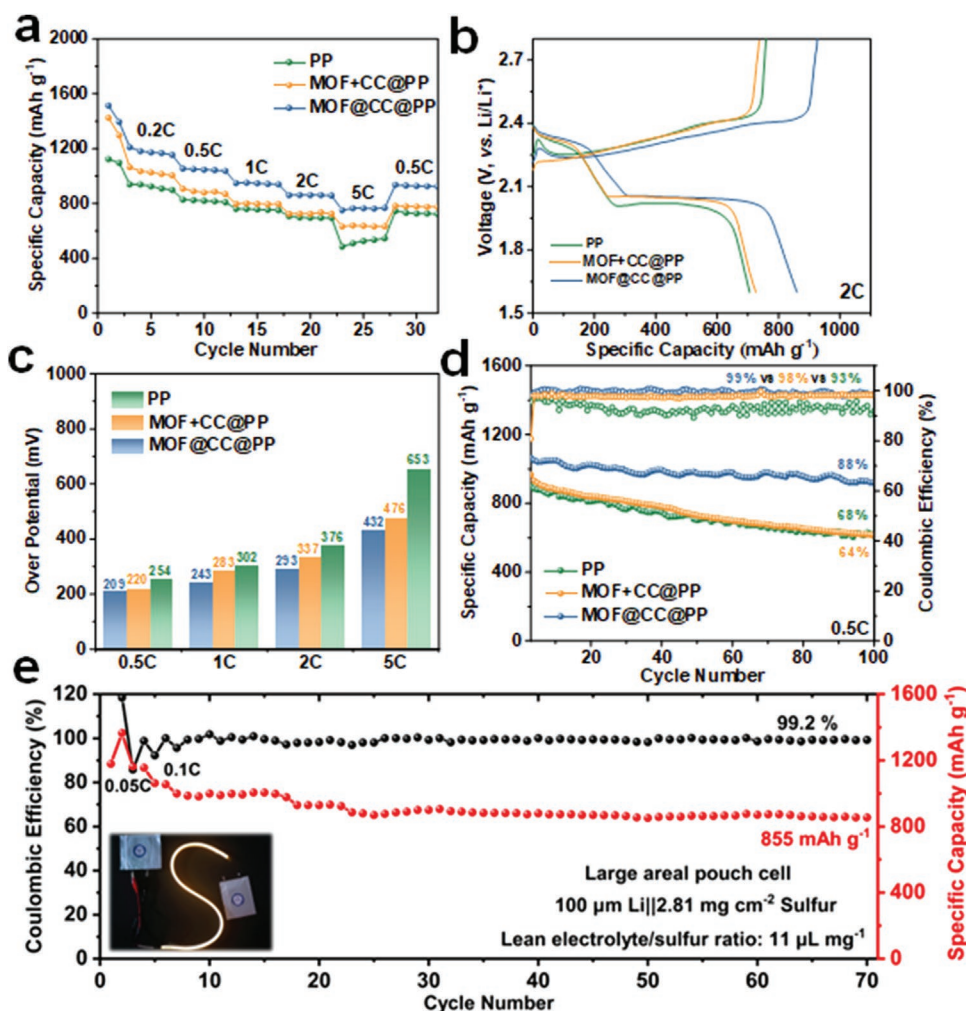


Figure 5. Electrochemical performance of Li/S full cells with MOF@CC kinetic promotor. a) Rate performances of Li/S batteries based on various separator with/without modification. b) The corresponding charge/discharge voltage curves at 2 C. c) The comparisons of overpotential cycled at different rates. d) Cycling performance with different separators at 0.5 C. e) Cycling performance of the large pouch cell using MOF@CC@PP under 2.81 mg cm⁻² at 0.1 C.

be achieved and it delivers a superior performance. The results suggest that the MOF@CC modified layer indeed enhances the performance of Li/S battery, and a homogeneous coating layer is crucial and herein 5 μm is suitable in current system.

To further evaluate the contribution of this MOF@CC layer on Li/S battery performance, a Li/S battery with a thin Li anode (the thickness of 50 μm) (Figure S23a, Supporting Information) and a high mass loading sulfur cathode (6.0 mg cm⁻²) was assembled (Figure S23b, Supporting Information). As shown in Figure S23c (Supporting Information), Li/S cell with MOF@CC@PP delivers a discharge capacity of 672 mAh g⁻¹ and Coulombic efficiency of 99.8% after 50 cycles at 0.3 C even under a low N/P ratio of 2.3, demonstrating that the cell can still achieve a satisfied performance with the assistance of MOF@CC in a high-loading cell. In the conditions of lean electrolyte (11 $\mu\text{L mg}^{-1}$) and the thickness of 100 μm Li, large areal pouch cell stabilizes cycling performance with a discharge capacity of 855 mAh g⁻¹ after 70 cycles and shows a high average CE of 99.2% (Figure 5e and Figure S24, Supporting

Information). More impressively, the MOF@CC layer presents a certain primary crystal structure and the surface morphology is still spherical particles after cycling (Figure S25, Supporting Information), indicating that MOF@CC layer keeps the catalytic functions.

3. Conclusion

In summary, a bridge-structured catalytic MOF@CC was proposed to regulate Li⁺ solvation structure, and thus improve Li⁺ diffusion, desolvation and redox reactions toward high sulfur reaction kinetics. Simulation and spectroscopic results confirm that Li⁺-solvents complex can be efficiently catalyzed by the bridged MOF@CC, creating a localized high lithium salt environment, which promotes the formation of anion-involved Li⁺ solvation structure or desolvated Li⁺. Benefited from these aggregated ion clusters, Li⁺ diffusion rate increases as evidenced by the calculated Li⁺ diffusion coefficients (D_{Li^+}).

Moreover, the C–N bridged bond simultaneously enhances ion and electron conduction for high catalytic efficiency, which dramatically reduce the aggregation and accumulation of polysulfides. With this catalytic MOF@CC@PP separator, a superior ionic conductivity (0.94 mS cm^{-1}) and a high Li⁺ transference number (0.66) are achieved. Consequently, the cell stabilizes 920 mAh g⁻¹ after 100 cycles at 0.5 C and a high rate performance reaches up to 765 mAh g⁻¹ at 5 C, much better than the controlled cells. Even under a low N/P ratio of 2.3, Li/S cell with MOF@CC@PP delivers a discharge capacity of 672 mAh g⁻¹ and Coulombic efficiency of 99.8% after 50 cycles at 0.3 C. In the pouch cell with 100 μm Li foil and the lean electrolyte, it can still deliver a discharge capacity of 855 mAh g⁻¹ after 70 cycles. We believe this work points out a new way to manipulate the Li⁺ solvation structure, which is critical in Li⁺ transport kinetics and the diffusion of polysulfides.

Supporting Information

Supporting Information is available from the Wiley Online Library or from the author.

Acknowledgements

L.L. and H.T. contributed equally to this work. The financial support from the National Key R&D Program (2021YFA1201503), National Natural Science Foundation of China (22075313; 21972164; 22279161), National Science Foundation of Jiangsu Province (BK. 20210130), the Innovative and Entrepreneurial Doctor in Jiangsu Province (JSSCBS20211428), Outstanding Youth Fund of Jiangxi Province (20192BCB23028), and Jiangxi Double Thousand Talent Program (JXSQ2019101072) is acknowledged. J. Wang also acknowledges the financial support by the Alexander von Humboldt Foundation and the basic funding of the Helmholtz Association.

Conflict of Interest

The authors declare no conflict of interest.

Data Availability Statement

The data that support the findings of this study are available from the corresponding author upon reasonable request.

Keywords

lithium sulfur batteries, lithium-ion transports, MOFs, polysulfide shuttle effects, solvation structures

Received: October 27, 2022

Revised: December 23, 2022

Published online: January 17, 2023

- [1] a) L. L. Jiang, C. Yan, Y. X. Yao, W. Cai, J. Q. Huang, Q. Zhang, *Angew. Chemie., Int. Ed.* **2021**, *60*, 3402; b) Q. Wu, Z. Yao, X. Zhou, J. Xu, F. Cao, C. Li, *ACS Nano* **2020**, *14*, 3365; c) Q. Wu, Z. Shadiki,

- J. Xu, F. Cao, C. Li, *Energy Storage Mater.* **2023**, *55*, 73; d) Y. Tong, S. Jin, H. Xu, J. Li, Z. Kong, H. Jin, H. Xu, *Adv. Sci.* **2022**, 2205443, <https://doi.org/10.1002/advs.202205443>.
 [2] a) G. Zeng, Y. Liu, D. Chen, C. Zhen, Y. Han, W. He, *Adv. Energy Mater.* **2021**, *11*, 2102058; b) Y. Liu, Y. Elias, J. Meng, D. Aurbach, R. Zou, D. Xia, Q. Pang, *Joule* **2021**, *5*, 2323; c) Q. Wu, Y. Zheng, X. Guan, J. Xu, F. Cao, C. Li, *Adv. Funct. Mater.* **2021**, *31*, 2101034; d) J. Wang, H. Hu, S. Duan, Q. Xiao, J. Zhang, H. Liu, Q. Kang, L. Jia, J. Yang, W. Xu, H. Fei, S. Cheng, L. Li, M. Liu, H. Lin, Y. Zhang, *Adv. Funct. Mater.* **2022**, *32*, 2110468; e) G. Zhou, H. Chen, Y. Cui, *Nat. Energy* **2022**, *7*, 312.
 [3] a) S. Cheng, J. Wang, S. Duan, J. Zhang, Q. Wang, Y. Zhang, L. Li, H. Liu, Q. Xiao, H. Lin, *Chem. Eng. J.* **2021**, *417*, 128172; b) J. Zhang, C. You, H. Lin, J. Wang, *Energy Environ. Mater.* **2021**, *5*, 731; c) S. Lopez, O. Akizu-Gardoki, E. Lizundia, *J. Clean Prod* **2021**, *282*, 124528; d) F. Lan, H. Zhang, J. Fan, Q. Xu, H. Li, Y. Min, *ACS Appl. Mater. Interfaces* **2021**, *13*, 2734; e) C. Li, Q. Zhang, J. Sheng, B. Chen, R. Gao, Z. Piao, X. Zhong, Z. Han, Y. Zhu, J. Wang, G. Zhou, H. M. Cheng, *Energy Environ. Sci.* **2022**, *15*, 4289.
 [4] a) Y. Huang, L. Lin, C. Zhang, L. Liu, Y. Li, Z. Qiao, J. Lin, Q. Wei, L. Wang, Q. Xie, D. L. Peng, *Adv. Sci.* **2022**, *9*, 2106004; b) S. Xin, L. Gu, N. H. Zhao, Y. X. Yin, L. J. Zhou, Y. G. Guo, L. J. Wan, J. *Am. Chem. Soc.* **2012**, *134*, 18510; c) G. Zheng, Y. Yang, J. J. Cha, S. S. Hong, Y. Cui, *Nano Lett.* **2011**, *11*, 4462; d) Z. Han, S. Zhao, J. Xiao, X. Zhong, J. Sheng, W. Lv, Q. Zhang, G. Zhou, H. M. Cheng, *Adv. Mater.* **2021**, *33*, 2105947.
 [5] a) B. Guo, S. Bandaru, C. Dai, H. Chen, Y. Zhang, Q. Xu, S. Bao, M. Chen, M. Xu, *ACS Appl. Mater. Interfaces* **2018**, *10*, 43707; b) H. Zhang, L. K. Ono, G. Tong, Y. Liu, Y. Qi, *Nat. Commun.* **2021**, *12*, 4738; c) W. Sun, C. Liu, Y. Li, S. Luo, S. Liu, X. Hong, K. Xie, Y. Liu, X. Tan, C. Zheng, *ACS Nano* **2019**, *13*, 12137; d) R. Gao, Q. Zhang, Y. Zhao, Z. Han, C. Sun, J. Sheng, X. Zhong, B. Chen, C. Li, S. Ni, Z. Piao, B. Li, G. Zhou, *Adv. Funct. Mater.* **2022**, *32*, 2110313.
 [6] a) J. Qian, W. A. Henderson, W. Xu, P. Bhattacharya, M. Engelhard, O. Borodin, J. G. Zhang, *Nat. Commun.* **2015**, *6*, 6362; b) H. Tu, L. Li, Z. Wang, J. Wang, H. Lin, M. Wang, C. Yan, M. Liu, *ACS Nano* **2022**, *16*, 16898.
 [7] a) H. Tu, L. Li, Y. Hu, Y. Zhang, Y. Wang, W. Huang, Z. Ren, H. Lin, M. Liu, *Chem. Eng. J.* **2022**, *434*, 134647; b) Z. Wang, H. Zhang, J. Xu, A. Pan, F. Zhang, L. Wang, R. Han, J. Hu, M. Liu, X. Wu, *Adv. Funct. Mater.* **2022**, *32*, 2112598.
 [8] a) Z. Wang, Y. Sun, Y. Mao, F. Zhang, L. Zheng, D. Fu, Y. Shen, J. Hu, H. Dong, J. Xu, X. Wu, *Energy Storage Mater.* **2020**, *30*, 228; b) Y. Hu, L. Li, H. Tu, X. Yi, J. Wang, J. Xu, W. Gong, H. Lin, X. Wu, M. Liu, *Adv. Funct. Mater.* **2022**, *32*, 2203336; c) Z. Yu, N. P. Balsara, O. Borodin, A. A. Gewirth, N. T. Hahn, E. J. Maginn, K. A. Persson, V. Srinivasan, M. F. Toney, K. Xu, K. R. Zavadil, L. A. Curtiss, L. Cheng, *ACS Energy Lett.* **2022**, *7*, 461.
 [9] a) Z. Chang, H. Yang, Y. Qiao, X. Zhu, P. He, H. Zhou, *Adv. Mater.* **2022**, *34*, 2201339; b) Z. Chang, Y. Qiao, H. Deng, H. Yang, P. He, H. Zhou, *Joule* **2020**, *4*, 1776; c) Z. Chang, H. Yang, X. Zhu, P. He, H. Zhou, *Nat. Commun.* **2022**, *13*, 1510; d) H. Yang, Y. Qiao, Z. Chang, P. He, H. Zhou, *Angew. Chemie., Int. Ed.* **2021**, *133*, 17867.
 [10] a) Z. Liang, J. Shen, X. Xu, F. Li, J. Liu, B. Yuan, Y. Yu, M. Zhu, *Adv. Mater.* **2022**, *34*, 2200102; b) H. Yang, L. Shang, Q. Zhang, R. Shi, G. I. Waterhouse, L. Gu, T. Zhang, *Nat. Commun.* **2019**, *10*, 4585.
 [11] a) J. Wang, L. Jia, J. Zhong, Q. Xiao, C. Wang, K. Zang, H. Liu, H. Zheng, J. Luo, J. Yang, H. Fan, W. Duan, Y. Wu, H. Lin, Y. Zhang, *Energy Storage Mater.* **2019**, *18*, 246; b) J. Wang, L. Jia, H. Lin, Y. Zhang, *ChemSusChem* **2020**, *13*, 3404.
 [12] a) J. Wang, S. Cheng, W. Li, L. Jia, Q. Xiao, Y. Hou, Z. Zheng, H. Li, S. Zhang, L. Zhou, M. Liu, H. Lin, Y. Zhang, *Nano Energy* **2017**, *40*, 390; b) X. Wang, G. Li, M. Li, R. Liu, H. Li, T. Li, M. Sun, Y. Deng,

- M. Feng, Z. Chen, *Energy Mater. Adv.* **2021**, *53*, 234; c) J. Wang, J. Zhang, S. Duan, T. Li, L. Jia, H. Liu, L. Li, S. Cheng, H. Hu, M. Huang, H. Hu, S. Zhang, Q. Xiao, H. Lin, *Chem. Eng. J.* **2022**, 429, 132352.
- [13] a) M. J. Dong, X. Wang, C. De Wu, *Adv. Funct. Mater.* **2020**, *30*, 1908519; b) R. Rong, Y. Sun, T. Ji, Y. Liu, *J. Memb. Sci.* **2020**, *610*, 118275.
- [14] S. Xu, L. Cai, P. Niu, Z. Li, L. Wei, G. Yao, C. Wang, F. Zheng, Q. Chen, *Carbon N Y* **2021**, *178*, 256.
- [15] J. Guo, Z. Yang, Y. Yu, H. D. Abruña, L. A. Archer, *J. Am. Chem. Soc.* **2013**, *135*, 763.
- [16] S. Zheng, X. Zhao, G. Liu, F. Wu, J. Li, *Nanotechnology* **2021**, *32*, 365404.
- [17] J. Rodríguez-Romero, J. Sanchez-Diaz, C. Echeverría-Arrondo, S. Masi, D. Esparza, E. M. Barea, I. Mora-Seró, *ACS Energy Lett.* **2020**, *5*, 1013.
- [18] a) Y. Xiao, W. Gong, S. Guo, Y. Ouyang, D. Li, X. Li, Q. Zeng, W. He, H. Deng, C. Tan, Q. Zhang, S. Huang, *ACS Mater. Lett.* **2021**, *3*, 1684; b) K. Xiao, J. Wang, Z. Chen, Y. Qian, Z. Liu, L. Zhang, X. Chen, J. Liu, X. Fan, Z. X. Shen, *Small* **2019**, *15*, 1901454; c) Q. Wu, Z. Yao, A. Du, H. Wu, M. Huang, J. Xu, F. Cao, C. Li, *J. Mater. Chem. A* **2021**, *9*, 5606; d) M. Huang, Z. Yao, Q. Yang, C. Li, *Angew. Chemie., Int. Ed.* **2021**, *133*, 14159.
- [19] a) L. Li, M. Wang, J. Wang, F. Ye, S. Wang, Y. Xu, J. Liu, G. Xu, Y. Zhang, Y. Zhang, C. Yan, N. V. Medhekar, M. Liu, Y. Zhang, *J. Mater. Chem. A* **2020**, *8*, 8033; b) Z. Wang, F. Zhang, Y. Sun, L. Zheng, Y. Shen, D. Fu, W. Li, A. Pan, L. Wang, J. Xu, J. Hu, X. Wu, *Adv. Energy Mater.* **2021**, *11*, 2003752.
- [20] J. Evans, C. A. Vincent, P. G. Bruce, *Polymer* **1987**, *28*, 2324.
- [21] a) S. Lee, K. Park, B. Koo, C. Park, M. Jang, H. Lee, H. Lee, *Adv. Funct. Mater.* **2020**, *30*, 2003132; b) J. F. Ding, R. Xu, N. Yao, X. Chen, Y. Xiao, Y. X. Yao, C. Yan, J. Xie, J. Q. Huang, *Angew. Chemie., Int. Ed.* **2021**, *60*, 11442; c) T. D. Pham, A. Bin Faheem, J. Kim, H. M. Oh, K. K. Lee, *Small* **2022**, *18*, 2107492.
- [22] a) C. Zhu, C. Sun, R. Li, S. Weng, L. Fan, X. Wang, L. Chen, M. Noked, X. Fan, *ACS Energy Lett.* **2022**, *7*, 1338; b) X. Chen, X. Zhang, H. Li, Q. Zhang, *Batter Supercaps* **2019**, *2*, 128.
- [23] a) Y. Jin, P. M. L. Le, P. Gao, Y. Xu, B. Xiao, M. H. Engelhard, X. Cao, T. D. Vo, J. Hu, L. Zhong, B. E. Matthews, R. Yi, C. Wang, X. Li, J. Liu, J. G. Zhang, *Nat. Energy* **2022**, *7*, 718; b) Y. Okamoto, S. Tsuzuki, R. Tatara, K. Ueno, K. Dokko, M. Watanabe, *J. Phys. Chem. C* **2020**, *124*, 4459.
- [24] a) A. Manthiram, Y. Fu, S. Chung, C. Zu, Y. Su, *Chem. Rev.* **2014**, *114*, 11751; b) M. Cuisinier, P. E. Cabelguen, S. Evers, G. He, M. Kolbeck, A. Garsuch, T. Bolin, M. Balasubramanian, L. F. Nazar, *J. Phys. Chem. Lett.* **2013**, *4*, 3227.
- [25] G. Liu, D. Luo, R. Gao, Y. Hu, A. Yu, Z. Chen, *Small* **2020**, *16*, 2005072.
- [26] J. L. Yang, S. X. Zhao, Y. M. Lu, X. T. Zeng, W. Lv, G. Z. Cao, *J. Mater. Chem. A* **2020**, *8*, 231.
- [27] S. D. Seo, C. Choi, D. Park, D. Y. Lee, S. Park, D. W. Kim, *Chem. Eng. J.* **2020**, *400*, 125959.
- [28] W. Zhao, Z. Pan, Y. Zhang, Y. Liu, H. Dou, Y. Shi, Z. Zuo, B. Zhang, J. Chen, X. Zhao, X. Yang, *Angew. Chemie., Int. Ed.* **2022**, *134*, e202205187.
- [29] a) H. Shi, X. Zhao, Z. S. Wu, Y. Dong, P. Lu, J. Chen, W. Ren, H. M. Cheng, X. Bao, *Nano Energy* **2019**, *60*, 743; b) B. Li, Q. Su, L. Yu, J. Zhang, G. Du, D. Wang, D. Han, M. Zhang, S. Ding, B. Xu, *ACS Nano* **2020**, *14*, 17285.
- [30] J. Zheng, G. Ji, X. Fan, J. Chen, Q. Li, H. Wang, Y. Yang, K. C. DeMella, S. R. Raghavan, C. Wang, *Adv. Energy Mater.* **2019**, *9*, 1803774.